ELSEVIER

Journal of Fluids and Structures 22 (2006) 897–903

JOURNAL OF FLUIDS AND STRUCTURES

www.elsevier.com/locate/jfs

On the force distribution along the axis of a flexible circular cylinder undergoing multi-mode vortex-induced vibrations

F.J. Huera Huarte[a,*], P.W. Bearman[a], J.R. Chaplin[b]

[a]*Department of Aeronautics, Imperial College London, Prince Consort Road, SW7 2BY London, UK*
[b]*School of Civil Engineering and the Environment, University of Southampton, Highfield, SO17 1BJ Southampton, UK*

Received 29 September 2005; accepted 8 April 2006
Available online 24 July 2006

Abstract

One of the main problems in predicting the response of flexible structures subjected to vortex shedding is that a totally reliable model for the fluid loading does not exist. It is also very difficult to measure the distributed force exerted by the fluid along the length of a marine riser without disturbing the system in some way. The methodology described here uses experimental response data obtained in a test programme undertaken in the Delta Flume in Holland during May 2003, linked to a finite element method model (FEM) of the riser. The length-to-diameter ratio of the model used was around 470, the mass ratio (mass/displaced mass) was 3 and the Reynolds number varied between 2800 and 28 000. By using the response data as the input to the numerical model, the instantaneous distributed in-line and transverse forces acting on a flexible cylinder can be studied.

Keywords: Vortex-induced vibration; Vortex shedding; Multi-mode response; Marine risers; Finite element method; Cylinder; Fluid loading on risers

1. Introduction

The prediction of the response of risers due to vortex-induced vibration is hindered by a lack of information on the fluid forces acting on a circular cylinder free to respond in many modes. Important progress has been made by measuring forces on a rigid section of a cylinder, either mounted on springs or forced to oscillate. Also forces have been calculated using CFD codes where in most cases the cylinder has been divided into a large number of segments and along each the flow is assumed to be two-dimensional. Evangelinos et al. (2000) have used a three-dimensional DNS code to determine fluid forces acting on a cylinder responding in its second mode: in one case as a standing wave and in the other as a travelling wave. They are not alone in commenting on the lack of any benchmark experiments that can be used to help validate their computational results. Measuring distributions of fluid forces acting on a flexible cylinder in a current, both in-line and transverse to the flow direction, is a challenging experimental problem. There are difficulties associated with having a large number of force transducers, achieving constant structural parameters of mass, damping and stiffness and preventing interference to the flow. In this paper, an indirect method of determining fluid forces is

*Corresponding author.
E-mail address: f.huera@imperial.ac.uk (F.J. Huera Huarte).
URL: http://www.imperial.ac.uk/people/p.bearman.

0889-9746/$ - see front matter
doi:10.1016/j.jfluidstructs.2006.04.014

described that uses displacements measured at a large number of points as input to a finite element model (FEM) of a flexible cylinder.

The input response data used comes from experiments by Chaplin et al. (2005), carried out on a model of a vertical tension riser exposed to a stepped current. The experiments were carried out at Delft Hydraulics in the Delta Flume, which was used as a towing tank. The flume is 230 m long, 5 m wide, and in these tests the water depth was 6.5 m. It is equipped with a heavy carriage whose maximum speed in either direction is 1.0 m/s. The model riser was 13.12 m long and had a diameter of 28 mm, giving a maximum Reynolds number of 28 000. The mass ratio, calculated as the mass of the model divided by the mass of fluid displaced, was 3 and the structural damping measured in free decay tests in air was around 0.3%. The effect of a stepped current was achieved by mounting the model on the towing carriage with the upper 55% of the model inside a chamber sealed at the top and with its other end open just below the water surface of the flume. By evacuating the air from the chamber, the upper 55% remained in still water while the lower 45% was exposed to a current. It was also possible to carry out tests with air completely filling the chamber. The response was determined from the outputs of strain gauges measuring bending in the in-line and transverse directions; 32 pairs of strain gauges were installed at a separation of 410 mm along the model length. The strain gauges nearest the extremities were placed at 205 mm from the ends. A tensioning device was placed at the top of the model, so the tension could be adjusted to avoid excessive axial stress. This consisted of an array of springs linking the fixed top end support with the top of the riser. Load cells were used to measure tensions and in-line forces at the top and bottom ends of the riser model.

The results from these experiments, including measured responses, are described by Chaplin et al. (2005). In the present paper these response measurements are used to obtain fluid forces, but the method devised can be equally well applied to other response data sets, so long as they have sufficient spatial resolution along the riser axis.

2. The numerical method

The marine riser model can be idealized as a beam with low flexural stiffness. The deflection of a generic beam is described by means of the Euler–Bernoulli beam equation. A Cartesian reference with its origin at the bottom of the riser has been used, in which the x axis is parallel to the flow velocity, z coincides with the vertical axis of the riser in its undeflected configuration and the y is perpendicular to both. The equation of motion of the riser is then

$$EI\frac{\partial^4 u_{x,y}(z,t)}{\partial z^4}-\frac{\partial}{\partial z}\left[T(z)\frac{\partial u_{x,y}(z,t)}{\partial z}\right]+c\frac{\partial u_{x,y}(z,t)}{\partial t}+m\frac{\partial^2 u_{x,y}(z,t)}{\partial t^2}=F_{T_{x,y}}(z,t), \tag{1}$$

where $u_{x,y}(z,t)$ is the deflection, m is the mass of the beam per unit length, c is the damping characteristic, EI is the flexural stiffness and $T(z)$ is the applied tension. The external fluid force is $F_{T_{x,y}}$ and all the fluid forces are included in the right-hand side of the equation. This equation neglects the effects of rotational inertia. The tension can be expressed as

$$T(z)=T_t-w(L-z), \tag{2}$$

T_t being the tension applied at the top of the riser, L the length of the riser and w the submerged weight. The model was pin-ended, hence displacements and curvatures were zero at each end, with the following boundary conditions:

$$\begin{aligned} &u(0,t)=0, \quad u(L,t)=0 \quad \forall t,\\ &\frac{\partial^2 u(0,t)}{\partial z^2}=0, \quad \frac{\partial^2 u(L,t)}{\partial z^2}=0 \quad \forall t. \end{aligned} \tag{3}$$

Using the finite element method, we transform Eq. (1) into a system of algebraic equations that gives the approximate solution of the equation in each finite element; see Masdemont-Soler (2002) or Bathe (1996). Extending this approximation to all the elements, and expressing it in matrix form, we obtain

$$\mathbf{KU}+\mathbf{C}\dot{\mathbf{U}}+\mathbf{M}\ddot{\mathbf{U}}=\mathbf{F}, \tag{4}$$

where $\mathbf{K}$ is the stiffness matrix, $\mathbf{C}$ the damping matrix, $\mathbf{M}$ the mass matrix and $\mathbf{U}$ the displacement vector. The overdot indicates differentiation with respect to time. Proportional or Rayleigh damping has been used, and this equates $\mathbf{C}$ as a linear combination of $\mathbf{M}$ and $\mathbf{K}$; i.e.,

$$\mathbf{C}=\alpha\mathbf{M}+\beta\mathbf{K} \quad (\alpha=0.0555,\ \beta=0.0002). \tag{5}$$

Coefficients α and β can be calculated using modal structural damping ratios and the natural frequency of the corresponding modes. Structural damping ratios were obtained from decay tests in air, assuming that the air damping was neglectable.

This linear model deals with cross-flow and in-line motions independently, and it does not consider axial components and the array of springs of the tensioning device at the top end of the cylinder. Two degrees of freedom are considered at each node of each element, one for the displacements $u_{x,y}(z,t)$ and the other for the slopes $\partial u_{x,y}(z,t)/\partial z$ (first spatial derivative of the displacements). With this method one can calculate the force distribution along the axis of the riser at each instant for which the displacements are available. This is done by putting the values of $\mathbf{U}$, $\dot{\mathbf{U}}$ and $\ddot{\mathbf{U}}$ into Eq. (4). Because deformations are relatively small compared to the length of the riser, a FEM linear model has been used for the in-line and cross-flow directions separately. Mass and stiffness matrices are constant in time and based on the initial static configuration with the vertical riser undeformed. Boundary conditions (3) are implicit in the measured values $\mathbf{U}$, and hence in $\dot{\mathbf{U}}$ and $\ddot{\mathbf{U}}$.

3. Force calculations

In some test cases the riser was submerged in water only up to 45% of its length. The rest was exposed to air and therefore the fluid forces on this part are expected to be very small compared to those on the lower half. Two representative test cases are presented here. One with the upper part exposed to water and the other with air.

The first case shown (May16_C021), in Figs. 1 and 2, is one of the experiments in which the riser was surrounded by water over its entire span. The flow speed was 0.85 m/s and the mean top tension during the steady part of the run was 1107 N. The Reynolds number was 23 800 and the reduced velocity, based on the fundamental natural frequency in still water of the riser at this tension, was 37.21. The reduced velocity based on the frequency of the dominant cross-flow mode was 5.72. The dominant cross-flow mode was the 7th running at a frequency of 5.33 Hz, and the dominant in-line mode was the 12th at 10.68 Hz.

Fig. 1 shows the in-line responses and force distributions as well as the r.m.s. (root mean square) of the in-line and the cross-flow response. In the upper left corner, the instantaneous in-line deflections with (Fig. 1(a)) and without (Fig. 1(b)) the mean deflected shape are shown for every half a second. The r.m.s. of the in-line motion is shown in the third plot (Fig. 1(c)). The distribution of local drag coefficient (C_d), appears in the fourth plot (Fig. 1(d)) also for every half second. The dashed lines mark the envelope of the drag distribution during the steady part of the run. The r.m.s. of the cross-flow motion is presented in Fig. 1(e) beside the C_d plot. The colour map (online) in the lower part of Fig. 1(g) shows the C_d distribution along the axis of the riser between the 30th and 40th second of the run. In the upper right corner (Fig. 1(f)) the C_d distribution appears expanded for the 36th second of the run.

Fig. 2 shows mainly the cross-flow forces for this first case. The upper left corner (Fig. 2(a)) shows the instantaneous cross-flow deflections. The r.m.s. of cross-flow (Fig. 2(b)) and in-line (Fig. 2(d)) motions are shown again, and finally the lift coefficient (C_l) distribution along the axis of the riser (Fig. 2(c)). Solid lines represent different instants half a second apart and the dashed lines the envelope of the C_l. The colour maps show the evolution in time of the C_l magnitudes for the same periods of time as in the previous figure. The vertical axes in Figs. 1–4 give the elevation from the bottom end of the riser to the top end at 13.12 m. The file Movie1.mpg included as an electronic annex, contains an animation showing in-line deflection, drag coefficient distribution, cross-flow deflection and lift coefficient distribution for this first case analyzed.

Results for the second example (May22_D006), with the upper part of the riser in air, can be seen in Figs. 3 and 4. The arrangement of the plots in these figures is the same as that explained for Figs. 1 and 2. In this case the flow speed was 0.85 m/s and the mean top tension was 2151 N, resulting in a reduced velocity based on the fundamental natural frequency of 24.20. The reduced velocity based on the frequency of the dominant cross-flow mode was 6.42. The Reynolds number was 23 800. The dominant cross-flow mode in this case was the 4th running at a frequency of 4.75 Hz, and in the in-line direction the 7th at 9.45 Hz. A second video, Movie2.mpg, showing this case is included as an electronic annex.

The inertial component of the force in Eq. (4), $\mathbf{M}\ddot{\mathbf{U}}$, has zero mean all along the axis of the riser and is in antiphase with respect to the stiffness part ($\mathbf{KU}$), which has zero mean only where the current profile is zero. The damping force ($\mathbf{C}\dot{\mathbf{U}}$) has been found to be very small compared to the other two components in (4). The contribution of the damping force to the total is less than 2%, hence damping forces can be neglected without significant loss of accuracy.

The figures show how in the lower half, the highest values of C_d are found at the positions where the cross-flow r.m.s. response is large. The C_d reaches peak values of around 4.5. In the upper part, the force is small even though the cross-flow r.m.s. response peaks have the same order of magnitude as in the lower part. It has been observed how in the case where the cross-flow deflection is large, the C_d distribution is not as uniform as it is when the cross-flow motions are small. At the nodes, C_ds tending to the stationary cylinder values at the Reynolds number of the experiments, are

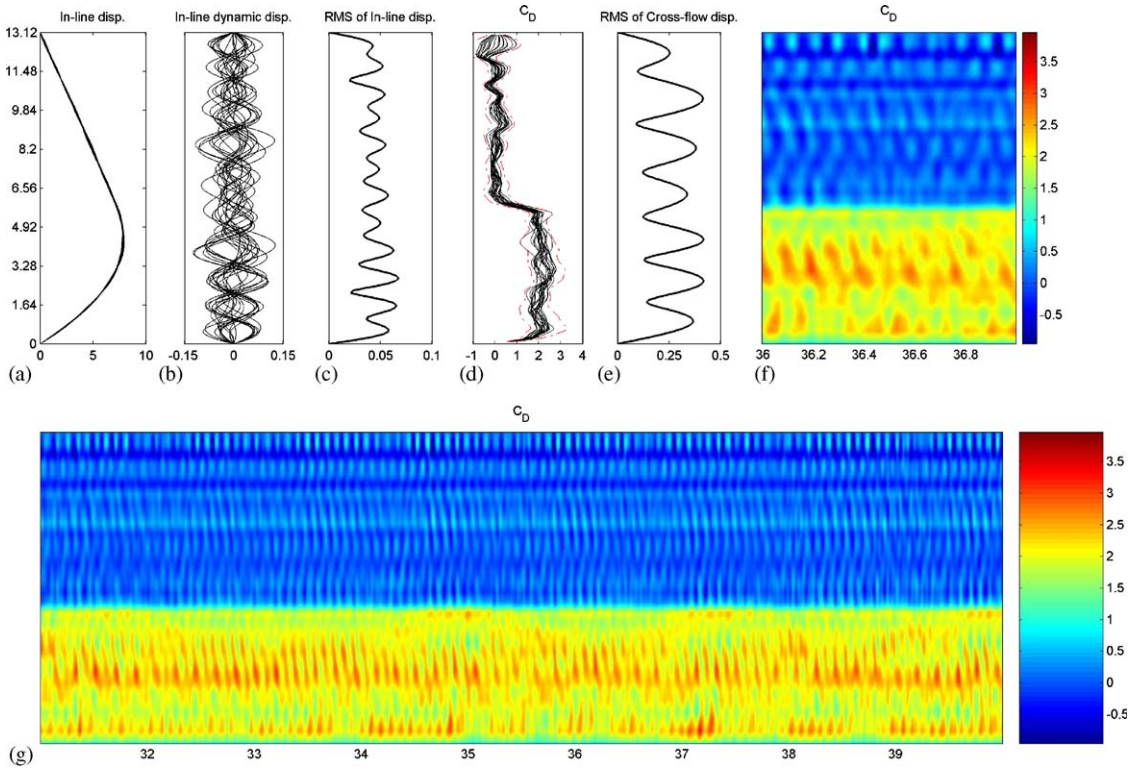

Fig. 1. Drag coefficient distribution—May16_C021.

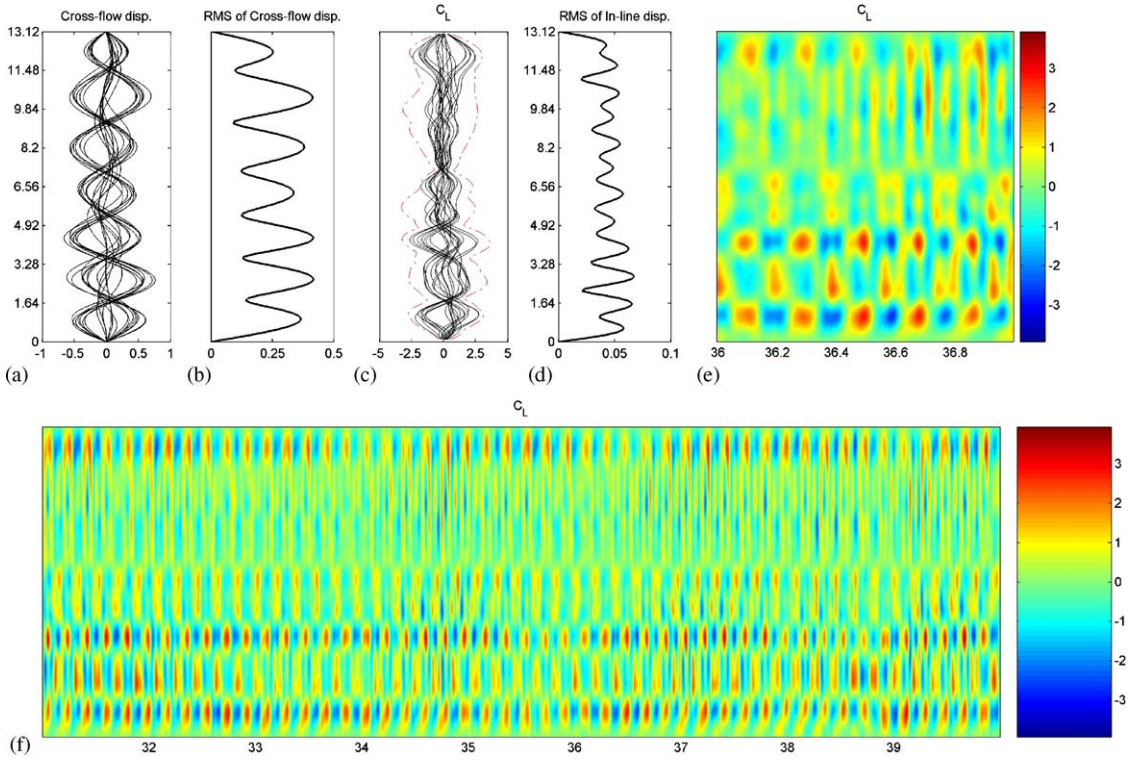

Fig. 2. Lift coefficient distribution—May16_C021.

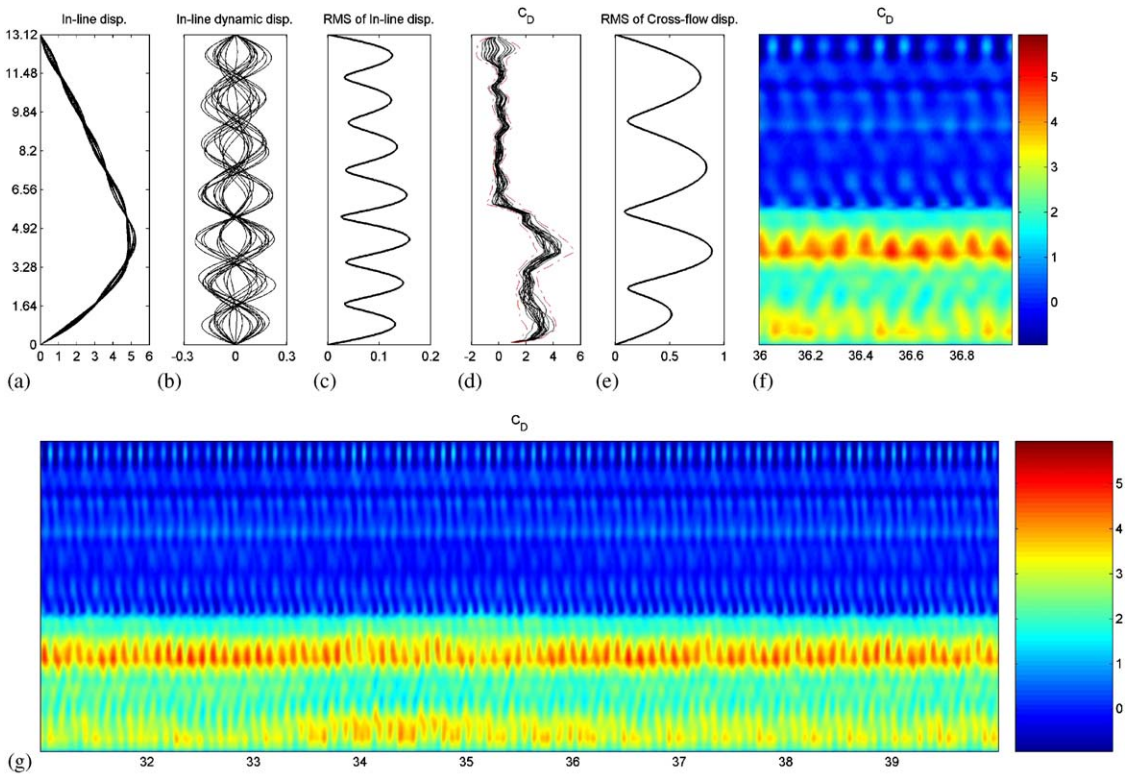

Fig. 3. Drag coefficient distribution—May22_D006.

observed. The lift distribution tends to follow the shape of the r.m.s. of the cross-flow motion. Local C_l peaks have been found with values up to 5, and these occur where the largest cross-flow deflections occur. The animations (Movie1.avi and Movie2.avi) made using this data suggest that in the lower part, where there is a uniform current, and the vortex shedding is exciting the riser model, the lift coefficient is close to being in phase with the motion. The lift at the nodes is practically zero, indicating that at these points, where the direction of the motion changes sign, vortex shedding is not occurring.

Measurements of force distributions for multi-modal vortex-induced vibrations are not available in the literature. However, similar high values of force coefficients, but for low Reynolds number and low mode number responses, have been observed by Evangelinos et al. (2000) in DNS computations. Although they only consider responses up to the second mode, many of the features of their results are similar to the ones presented here.

Mean drag coefficients based on the riser length exposed to the current, for all the test cases, have been computed using the methodology described here. They are shown in Fig. 5 as open circles. The total drag forces that have produced these drag coefficients have been calculated as the spatial integration of the in-line force distribution over a period of 30 s for most of the cases. The filled circles in Fig. 5 are the experimental drag coefficients obtained from the load cell signals at the ends of the model. They have been calculated by resolving the measured tension in the in-line direction. Solid lines mark the different lock-in regions, and over them the dominant cross-flow/in-line mode is indicated. Lines along the reduced velocity axis, indicate the various lock-in regions. In this figure, the drag coefficients for those experimental runs where the upper half of the riser was in air rather than in water, are also plotted. It can be seen how the C_ds obtained through the methodology presented here are very close to the values found using the direct measurement method.

The noise in the measured signals, the fact that the array of springs at the top of the model has not been modelled and the use of the initial configuration geometry to calculate the stiffness, mass and damping matrices, which are not updated each time step, are believed to be the main sources of error. An error estimation in the force distribution calculations, can be done by looking to the cases with the upper half length in air, in which the expected hydrodynamic forces should be practically zero. The force coefficient maximum values found in the upper part for these cases are

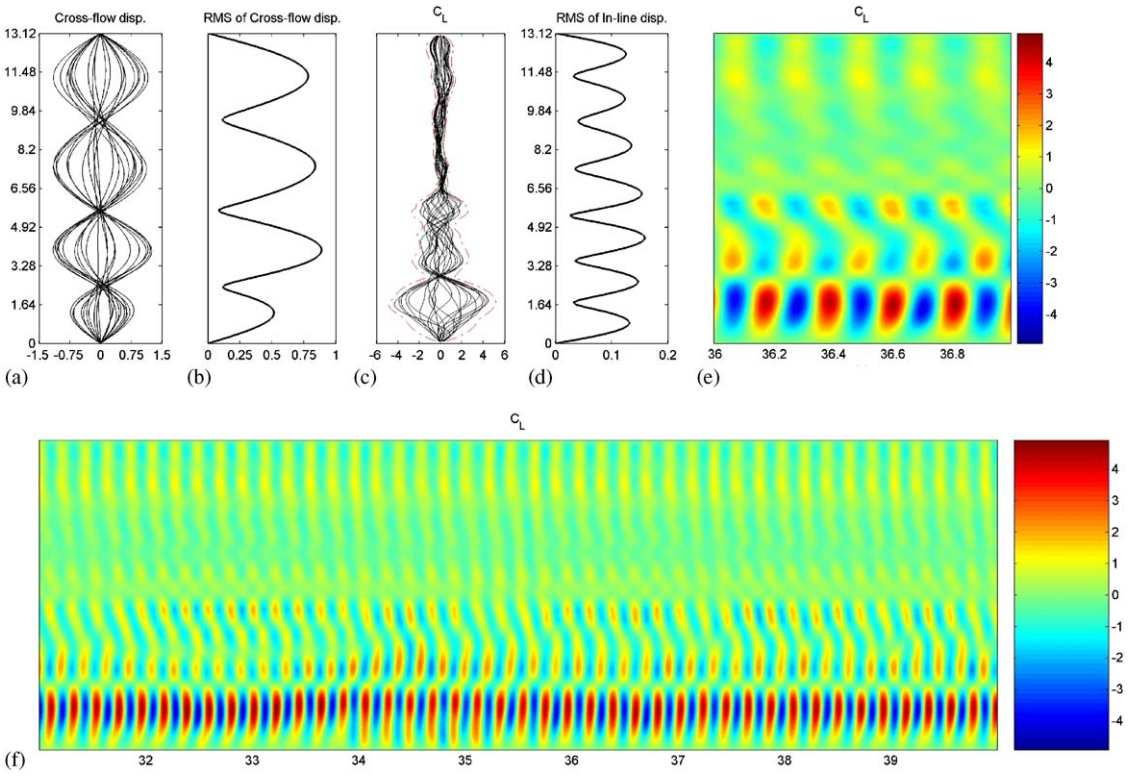

Fig. 4. Lift coefficient distribution—May22_D006.

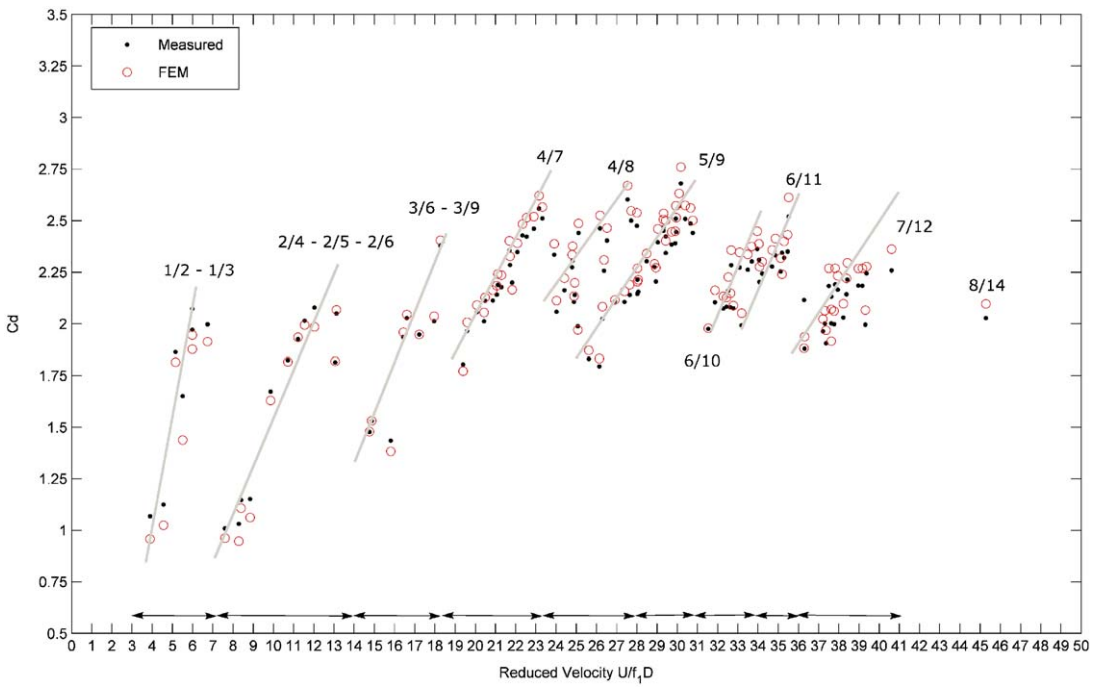

Fig. 5. Measured and calculated C_d coefficients.

approximately 15% of the maximums resulting in the lower part. In the top end, where the array of springs is located, the error has been found to be higher than 15%.

4. Conclusions

The time-dependent fluid force distribution on a vertical tension riser model undergoing vortex-induced vibrations in a stepped current, has been obtained from measured displacements by an indirect finite element technique.

The drag distributions tend to follow the shape of r.m.s. cross-flow deflection, revealing quantitatively the increase in drag that occurs where cross-flow deflections are the largest. In cases with large cross-flow response the drag distributions along the riser have been found to be quite variable, contrary to what happens with low cross-flow responses. Local instantaneous C_d values up to 4.5 have been found. At the nodes, where practically no response is found, values of C_d approaching those of stationary cylinders at the Reynolds number of the experiment have been observed.

Computed distributions of the C_l also tend to follow the form of r.m.s. cross-flow deflections, with very small values at the nodes, and maximum values of C_l up to 5 at anti-nodes. Animations generated with these data suggest that the lift force is almost in phase with the deflection of the model in the regions where the riser is exposed to a current.

This methodology and the resulting data, of which this paper shows only two examples, may contribute to an improved understanding of vortex-induced vibrations. They also provide new opportunities for validating flow-induced forces computed by CFD coupled with structural codes.

Acknowledgements

This work was supported by EPSRC, by the European Commission through the Large Facilities programme, and by BP.

Appendix A. Supplementary data

Supplementary data associated with this article can be found in the online version, at 10.1016/j.jfluidstructs.2006.04.014

References

Bathe, K.J., 1996. Finite Element Procedures, second ed. Prentice-Hall, Englewood Cliffs, NJ.

Chaplin, J.R., Bearman, P.W., Huera-Huarte, F.J., Pattenden, R., 2005. Laboratory measurements of vortex-induced vibrations of a vertical tension riser in a stepped current. Journal of Fluids and Structures 21, 3–24.

Evangelinos, C., Lucor, D., Karniadakis, G.E., 2000. Dns-derived force distribution on flexible cylinders subject to vortex-induced vibration. Journal of Fluids and Structures 14, 429–440.

Masdemont-Soler, J., 2002. Curs d'elements finits amb aplicacions, first ed. Politext Edicions UPC, Technical University of Catalonia.